Behavior of n = 1 magnetohydrodynamic modes of infernal type at high-mode pedestal with plasma rotation

L. J. Zheng, M. T. Kotschenreuther, and P. Valanju
Institute for Fusion Studies, University of Texas at Austin, Austin, Texas 78712, USA

(Received 26 September 2012; accepted 13 December 2012; published online 3 January 2013)

Magnetohydrodynamic instabilities of high-mode (H-mode) pedestal are investigated in this paper with the inclusion of bootstrap current for equilibrium and rotation for stability. The jointed European torus-like equilibria of H-mode discharges are generated numerically using the VMEC code. It is found that, when the bootstrap current is taken into account, a safety-factor reversal or plateau can be generated near plasma edge. This confirms previous results of numerical equilibrium reconstructions using other types of codes. The $n = 1$ magnetohydrodynamic instabilities, where n is toroidal mode number, are investigated numerically in this type of equilibria using the AEGIS code. It is found that the infernal type harmonic can prevail at safety-factor reversal or plateau region. The toroidal plasma rotation effect with low Mach number is investigated. The numerical results show that the mode frequency is close to the rotation frequency at pedestal top, when the value of safety factor at plateau is slightly above a rational number. This mode frequency range seems to coincide with the experimentally observed frequencies of $n = 1$ edge harmonic oscillations (or outer modes) at the quiescent H-mode discharges. © *2013 American Institute of Physics*.
[http://dx.doi.org/10.1063/1.4773898]

I. INTRODUCTION

Since being found in the 1980s, the H-mode—an operating mode with high energy confinement[1]—has today been adopted as a reference for next generation tokamaks, especially for ITER. However, the H-mode confinement is often tied to the damaging edge localized modes (ELMs).[1] There is a concern that ELMs can potentially damage divertor plates, due to the discharged heat load. This is particularly the case for big devices like ITER. While various solutions are proposed, an interesting solution is to develop the so-called quiescent H-mode (QH-mode).[2] ELMs are avoided in QH-mode. As a distinguishing feature, QH-modes are always accompanied by the excitation of the so-called edge harmonic oscillations (EHOs) or outer modes (OMs).[2,3] In contrast to ELMs, EHOs (or OMs) are mild magnetohydrodynamic (MHD) activities, which can pump out plasma energy steadily without damaging the divertors. Therefore, it is interesting to investigate the stability of QH mode and to find out the possible explanation for EHOs (or OMs).

The investigation of equilibrium and stability of QH-modes is theoretically challenging. The existence of edge transport barrier at QH-mode confinement is the main cause of complications. The transport barrier results in a pedestal region near plasma edge, where the pressure gradient is steep. In the pedestal region, the bootstrap current density can be comparable or even larger than the Ohmic current density.

Previously, the peeling or kink/peeling modes are proposed to explain EHOs or OMs.[4,5] Note that QH mode usually occurs at hot temperature or low density discharges, where the collisionality is low. As is well known, the bootstrap current increases as the collisonality decreases. Strong bootstrap current in the low collisionality regime may lead the safety factor profile to reverse or to form a plateau (referred to as q plateau) in the pedestal region. Several recent works point to the likelihood that low collisionality QH mode pedestals have a flat spot or plateau in the q profile.[6] This leads to flourishing investigations to study the stability of this type of equilibria,[7–9] including the current work that proves the existence of infernal modes.

It is possible that different mechanisms are dominant in different regimes. For regimes where EHO is observed without a plateau in the q profile, the kink/peeling interpretation may be likely. However, if the EHO is observed where there is a flat spot in the q profile, we believe an interpretation in terms of infernal modes is favored.

The measurement of safety factor profile at plasma edge is challenging for current diagnostics techniques. Numerical reconstructions are used to get the safety factor profile.[6–9] We study the jointed European torus (JET)-like equilibrium of QH-mode discharges. Note that QH mode occurs at the low collisionality regime. This leads us to generate the numerical equilibria using the VMEC code with low collisonality bootstrap current model.[13] We investigate the MHD instabilities in this type of equilibria using AEGIS code,[14] with the effects of the low-Mach-number rotation being taken into consideration in the mode calculation.[15]

The qualitative change in the safety factor profile can significantly modify the MHD mode behavior. MHD modes of the infernal mode type[10,11] can prevail at the region where the safety factor has a plateau or is reversed. Infernal mode is quite different from the peeling-ballooning modes.[4,5] Snaky-type modes in internal transport barriers with flat q profiles have been interpreted as infernal modes.[12] This further motivates us to study the infernal modes as an explanation of snaky type phenomenon in the pedestal.

Another reason for us to infer that EHOs (or OMs) may be infernal modes is due to their typical frequencies: for

$n = 1$ modes the frequency is the rotation frequency near the pedestal top. For $n > 1$ modes, the frequencies are the n multiple of $n = 1$ mode frequency. As is well known, for a pure peeling mode, theory gives nearly zero mode frequency. This disqualifies it as the EHO (or OM) candidate. Reference 4 instead considers the kink/peeling modes as candidate. However, a kink mode has multiple resonances and the rotation frequency is different on each surface. It again cannot necessarily explain why EHO frequency takes the rotation frequency near pedestal top. Our physics intuition leads us to consider the infernal modes, which has a mode structure to pickup the rotation frequency near the pedestal top as the $n = 1$ mode frequency, as found in experiments. As will be discussed later in the paper, the $n > 1$ infernal modes also pick up the n multiple of the rotation frequency near the pedestal top as their mode frequencies.

Experimental observations show that ELMs always induce the scrape-off-layer (SOL) current.[16] One can anticipate that a positive feedback of such a SOL current to the MHD modes at pedestal can lead to a nonlinear amplification of MHD activities. This process has been used to interpret the explosive growth of ELMs.[17] Strong coupling to SOL currents obviously relates to external modes. Apparently, the EHOs (or OMs) do not grow to large amplitude, and their coupling to SOL is weak. This suggests that EHOs (or OMs) may relate to internal modes. Infernal modes at pedestal fit these two mode features. Also, taking into account the strong bootstrap current effect at low collisionality, somewhat near the pedestal top, a flat region appears in q. Consequently, the infernal modes appear naturally, as can be seen from the calculations later on in this paper. This, then, leads us to consider them as potential candidates for EHOs (or OMs).

This paper is arranged as follows: In Sec. II, the numerical equilibria for JET-like configuration are described and the numerical scheme for stability analyses upon these equilibria is presented; In Sec. III, the linear stability analyses for the cases without rotation are given; In Sec. IV, the linear stability analyses for the cases with rotation are presented; conclusions and discussion are given in the last section.

II. EQUILIBRIUM AND NUMERICAL SCHEME

In this section, we describe the generation of numerical equilibria for JET-like configuration and present the numerical scheme for the stability investigation of these equilibria with the inclusion of plasma rotation effects.

To be specific we focus our investigation on the JET-like H-mode discharges. The equilibria are generated numerically using the VMEC code.[13] The plasma cross section is shown in Fig. 1. This plot uses the VMEC code grid. In the stability calculation re-griding is performed. Especially, denser grid points are packed at rational surfaces in the radial direction, in order to resolve continuum damping. The VMEC code we use computes the bootstrap current in the collisionless limit, which is appropriate for the low collisionality ($\nu_* \to 0$) plasmas. We use the STELLOPT[18] code (part of the VMEC code suite) to compute the collisionless limit of the bootstrap current.[19] For parameters typical of

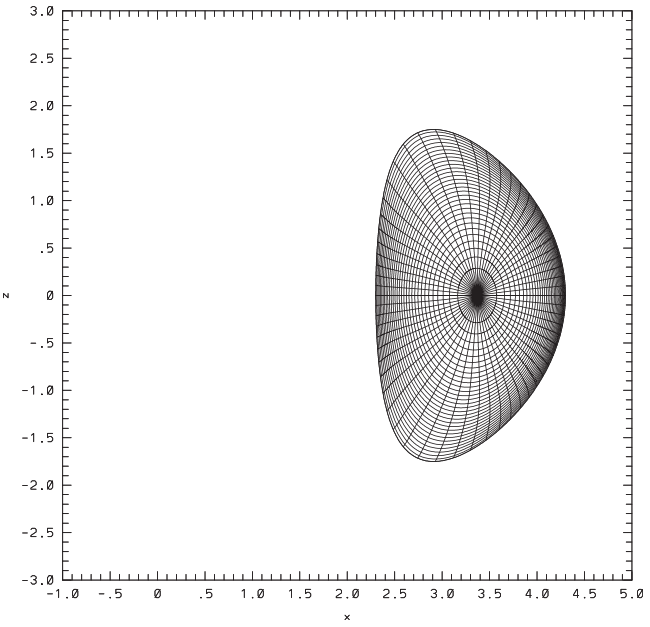

FIG. 1. Cross section of JET-like configuration. The horizontal coordinate X represents the distance from axisymmetric axis. The vertical coordinate Y is the height from the vertical mid-plane. Conformal wall is assumed.

QH mode pedestals ($v^* = 0.05$ and $r/R = 0.3$), the bootstrap current is approximately 80%-90% of the collisionless limit.[20] In addition, numerical calculations find that there are modest modifications due to finite poloidal gyroradius[20] (which have yet to be evaluated for QH modes). Therefore, our equilibrium employs a current spike in the pedestal which is in the range of 85%-90% of the collisionless bootstrap current. For the equilibrium here, a flat spot in the q profile is found for a current spike with a peak value of 88% of the peak value of the collisionless bootstrap current.

We use conformal wall in the calculation. We also point out that the rotation effects on the equilibrium are not included in our calculation. The rotation effects on equilibrium are of order of the square of the ratio between the rotation speed and ion thermal speed. For subsonic rotation investigated in this paper, they are small and therefore can be neglected.[21,22]

The steep pressure gradient at pedestal region can induce the bootstrap current at that region. Taking into account the bootstrap current in the equilibrium calculation, it is found that a safety-factor (q) reversal or plateau can indeed appear in the pedestal region. The equilibrium results are consistent to the previous calculations with other codes as given in Ref. 6. We denote the safety factor value at plateau as q_p.

In order to study the difference between the cases with q_p larger and smaller than an integer number. We generate five different equilibria for stability analyses, with the safety factor at plateau, q_p, ranging from 4.2, 4.1, 4, 3.96, to 3.92. The safety factor profiles are plotted in Fig. 2; while the corresponding pressure profiles are plotted in Fig. 3. The correspondence between five pressure and safety factor profiles is up-down reversed in Figs. 2 and 3. We keep the five equilibria to have the same beta normal, though their pressure profiles are slightly different. We have not considered further

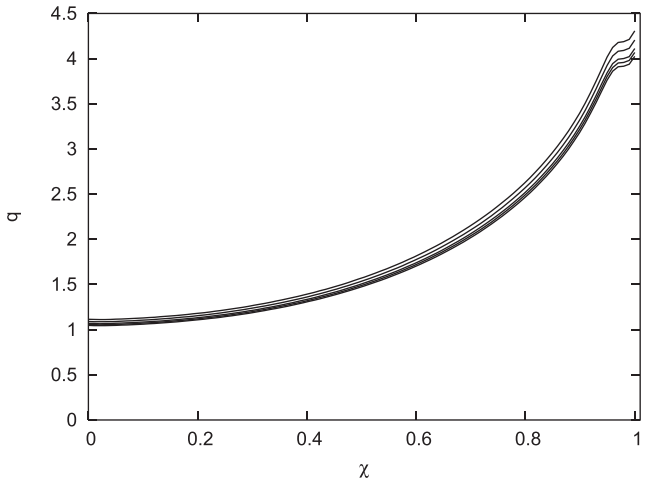

FIG. 2. Safety factor profiles versus normalized poloidal magnetic flux. The safety factor values at the plateau range from 4.2, 4.1, 4, 3.96, to 3.92 top-down.

lower q_p case, in order to avoid the edge q value to fall below 4, which represents a qualitative change of equilibrium properties. Like in Ref. 6, the VMEC code does not include the x-point effect. Consequently, the edge q value is underestimated. The x-point effects will be considered in the future. In Fig. 3, the pressure is normalized by μ_0/B_0^2, where B_0 is the magnetic field at magnetic axis. We assume that rotation is sub-sonic and therefore its effect on equilibrium is negligible, as compared to thermal pressure effects. The rotation profiles are assumed to be the same as the pressure ones. Density also enters the MHD equation through inertia effect. Since the measurements of density profiles in the pedestal contain uncertainty, we use the most conservative profile to estimate the rotation effects at the pedestal, by assuming that the density has the same profile as pressure. This would assure there is no overestimate of the inertia term, which contains the rotation effects, at the pedestal.

As one can imagine, the appearance of safety factor plateau can destroy the local ballooning invariance, so that the

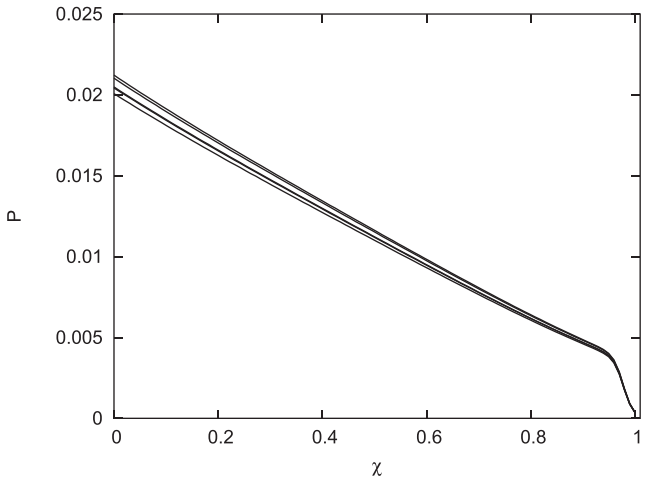

FIG. 3. Pressure profiles versus normalized poloidal magnetic flux. Pressure is normalized by the magnetic pressure at magnetic axis. The pressure profiles correspond to the safety factor profiles in Fig. 2 with $q_p = 4.2$, 4.1, 4, 3.96, and 3.92 bottom-up. The curve for $q_p = 4$ is only slightly above that for $q = 4.1$.

peeling-ballooning type of modes in the normal shear case becomes modified. Especially, the safety factor plateau can minimize the magnetic shear stabilization and cause the "fat interchange modes" (i.e., infernal modes) to develop locally.[10,11]

To confirm this observation, the MHD instabilities in this type of equilibria are investigated numerically using the AEGIS code.[14] The adaptive numerical scheme of AEGIS code allows us to study the rotation-induced continuum damping.[15] We limit ourselves to consider $n = 1$ modes in this paper, where n is toroidal mode number. The basic MHD equation used for our stability analyses is as follows:

$$-\rho_m \hat{\omega}^2 \boldsymbol{\xi} = \delta\mathbf{J} \times \mathbf{B} + \mathbf{J} \times \delta\mathbf{B} - \nabla\delta P, \tag{1}$$

where $\boldsymbol{\xi}$ is the perpendicular field line displacement, $\mathbf{B}$ denotes equilibrium magnetic field, the perturbed quantities are tagged with δ, the perturbed magnetic field $\delta\mathbf{B} = \nabla \times \boldsymbol{\xi} \times \mathbf{B}$ is perturbed magnetic field, $\mathbf{J}$ is equilibrium current density, $\delta\mathbf{J} = \nabla \times \delta\mathbf{B}$ is perturbed current density, P represents the equilibrium pressure, $\delta P = -\boldsymbol{\xi} \cdot \nabla P$ is the perturbed pressure of convective part, ρ_m is the mass density, $\hat{\omega} \equiv \omega + n\Omega$, and Ω represents toroidal rotation frequency. The plasma compressibility effect is not included formally. However, since the mode frequencies we are studying are much smaller than the ion acoustic wave frequency, the plasma compressibility results only in the so-called apparent mass effect, as proved in Ref. 23. Therefore, we include the plasma compressibility effect by regarding ρ_m as the total mass, i.e., the summation of perpendicular mass and parallel mass (i.e., apparent mass in the perpendicular momentum equation). Since rotation frequency is assumed to be much lower than the ion acoustic frequency, we then include the rotational effects through a Doppler shift in our formalism. Rotation effects enter into the problem in three categories—that is, not only through the Doppler shift but also via centrifugal force and Coriolis force. For the case with the rotation speed being much less than the ion thermal speed, however, it can be shown that the rotational effects of centrifugal force and Coriolis force are negligible.[21,22] Consequently, we can keep the rotational effects only from the Doppler shift.

Experimental observations both in DIII-D and JET show that EHOs (or OMs) have finite frequencies, about 10 kHz for $n = 1$ modes.[2,3] For modes with such high frequencies, the conductor wall surrounding plasma torus behaves as a perfectly conducting wall. Therefore, our calculations focus only on the perfectly conducting wall case.

Furthermore, EHOs (or OMs) are purely oscillating modes with zero or very small growth rate. We need to compute the marginal stability case. As is well-known, in the marginal or nearly marginal stability case, the MHD equation, Eq. (1), is singular. One needs to consider the analytical continuation to the complex plane, so that the singularity can be avoided on the integration path, similar to the computation of Landau damping in the velocity space. To avoid the complication of analytical continuation of MHD equation, we instead use an alternative approach by analytical continuation of dispersion relation $D(\omega)$ to determine the roots near

marginal stability. This includes both zero and small growth rate roots. Similar technique has been successfully used in calculating Alfvén modes in the continuum using the AEGIS code.[24] This is based on the Cauchy-Riemann condition for an analytical function, which in this case is the complex dispersion relation $D(\omega)$ with argument $\omega = \omega_r + i\omega_i$:

$$\frac{\partial D_r}{\partial \omega_r} = \frac{\partial D_i}{\partial \omega_i}, \tag{2}$$

$$\frac{\partial D_i}{\partial \omega_r} = -\frac{\partial D_r}{\partial \omega_i}, \tag{3}$$

where subscripts r and i represent, respectively, real and imaginary parts. According to the Cauchy-Riemann condition, an analytical function can be fully determined in the whole complex plane by its value in a piece of complex domain, for example, by the value on a line. In our application of this mathematical theorem, we compute $D(\omega_r + i\omega_i)$ for a domain of ω_r at given ω_i. In this case, the derivatives on the left hand sides of Eqs. (2) and (3) are computed and therefore those derivatives on the right are determined as well. Subsequently, the derivatives on the right hand sides can be used to push a step toward $\omega_i + \delta\omega_i$, with $\delta\omega_i/\omega_i \ll 1$ for each ω_r. Afterward, $D(\omega_r + i(\omega_i + \delta\omega_i))$ is determined. Repeating this kind of procedures one can get $D(\omega_r + i\omega_i)$ in whole domain. In practice, we use Chebyshev polynomial for fitting to get smooth derivatives. As we know, a MHD code can compute $D(\omega_r + i\omega_i)$ for a given positive ω_i without encountering singularities. The AEGIS code uses an adaptive scheme and therefore the positive ω_i can be chosen to be very small. This reduces considerably the range of analytical continuation for dispersion relation. The unstable roots from this method can be verified by the AEGIS code.

III. MHD INSTABILITIES WITHOUT ROTATION

In this section, we study the case without plasma rotation. We investigate the $n = 1$ modes. Figure 4 shows the critical wall positions for five different equilibria with safety factor and pressure profiles given in Figs. 2 and 3.

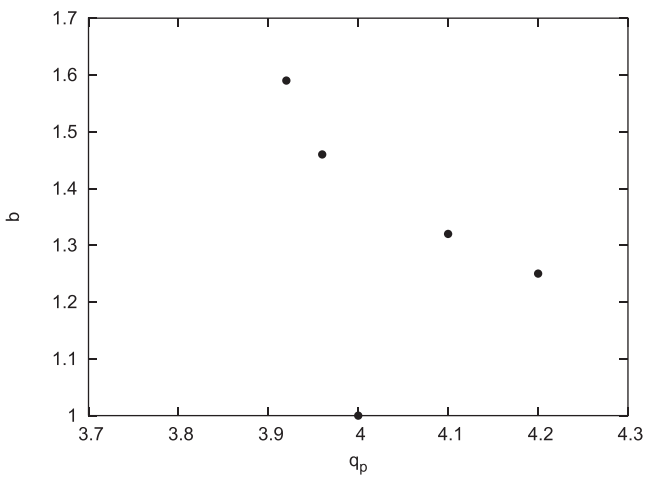

FIG. 4. The critical wall position versus the safety factor value at q plateau. Five cases corresponding to the safety and pressure profiles in Figs. 2 and 3 are shown.

First, we note that the $q_p = 4$ case is Mercier-unstable. This case is therefore unstable to the fixed boundary modes and its critical wall position falls to 1. Its eigen function is simply a delta-function-like peak at the resonance point for a single Fourier component. The corresponding marginally stable eigenfunctions for the cases with q_p being 4.1 and 3.96 in Fig. 1 are plotted, respectively, in Figs. 5 and 6. We can find from Figs. 5 and 6 that the $m = 4$ harmonic is substantially different from other harmonics, for example, $m = 2$ and 3 harmonics. The $m = 2$ and 3 components tend to changes abruptly at the mode rational surfaces. However, the $m = 4$ component is shifted toward the low shear region and is "fat." It exhibits the typical infernal mode feature.[10,11] This is understandable, because in the low shear region the magnetic shear stabilization is minimized, but the pressure drive is enhanced due to the steep pressure gradient at pedestal region.

From Fig. 4, one can find that the cases with q_p smaller than 4 have larger critical wall positions—i.e., are more stable—than the cases with q_p larger than 4. Examining the two eigen modes figures and q profiles in Figs. 5 and 6, one can find that the $m = 4$ resonance surface in the case with $q_p = 3.96$ is much closer to the plasma-vacuum interface than the $q_p = 4.1$ case. If the peeling-ballooning modes dominated, the $q_p = 3.96$ case would be more unstable. However, since it is dominated by the internal energy balance, the local equilibrium properties for infernal harmonic $m = 4$ determine the stability criterion. Because the pressure gradient around the pedestal top is larger than that at pedestal foot—that affects the $m = 4$ harmonic, the $q_p = 4.1$ case becomes more unstable than the $q_p = 3.96$ case. This infernal mode feature becomes even more evident when the rotation effects are taken into consideration in Sec. IV.

We also find that the MHD instabilities of such a type of equilibria are sensitive to the distance of q plateau to the plasma edge. The closer to the plasma edge the q plateau is, the more unstable the system becomes.

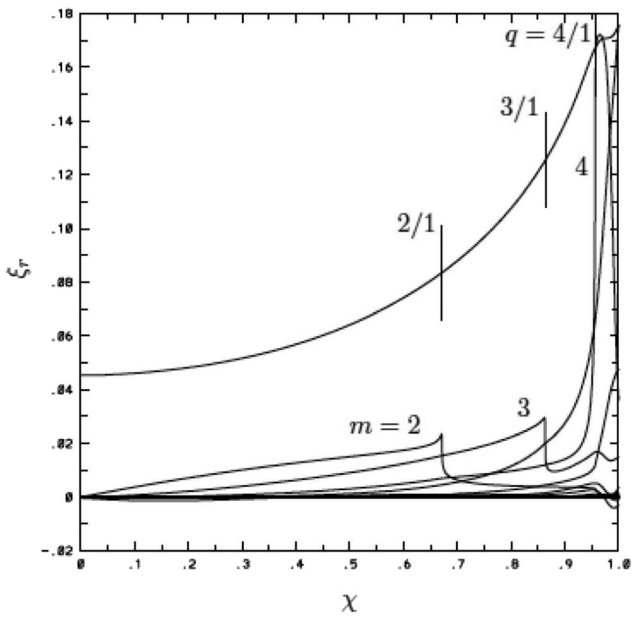

FIG. 5. The eigenfunction versus normalized poloidal magnetic flux for the case with $q_p = 4.1$, $b = 1.33$, and $\Omega = 0$.

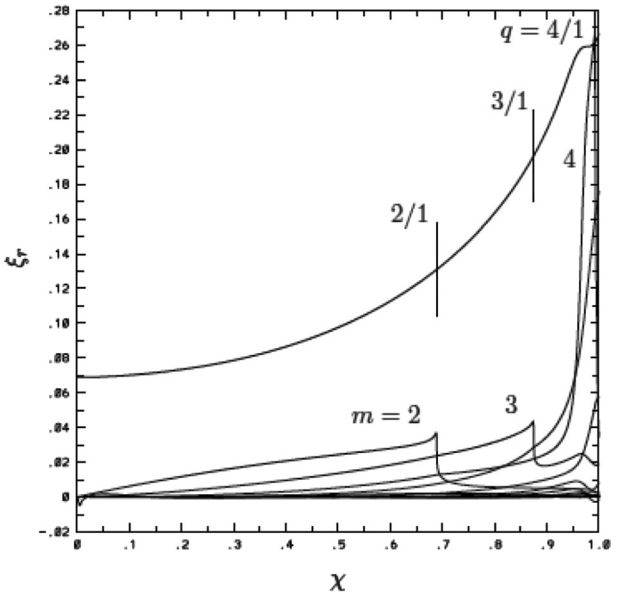

FIG. 6. The eigenfunction versus normalized poloidal magnetic flux for the case with $q_p = 3.96$, $b = 1.47$, and $\Omega = 0$.

IV. MHD INSTABILITIES WITH ROTATION

In this section, we investigate the rotation effects on the equilibria studied in the last section. This is interesting, because the EHOs (or OMs) as observed experimentally have finite frequencies. Noting that the EHO frequencies are high, well above the typical resistive wall mode frequency, we only need to compute the ideal wall case. This investigation can further confirm the infernal mode features and help clarifying the possible connection with the experimental observations of EHOs (or OMs).

To be specific, let us discuss two cases: one with q_p larger than 4 and the other less than 4. The eigen frequency and growth rate versus the wall position b for the $q_p = 4.1$ case are plotted in Fig. 7, with the central rotation frequency Ω normalized by the Alfvén frequency at magnetic axis as parameter; while those for the $q_p = 3.96$ case are plotted in

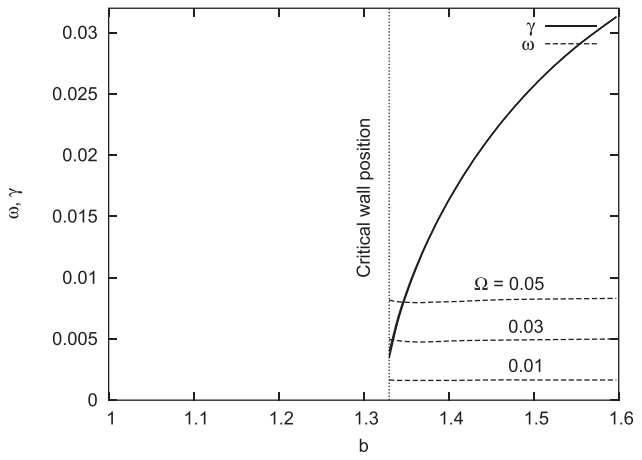

FIG. 7. The eigen frequency ω and growth rate γ versus the wall position b for the case with $q_p = 4.1$. The normalized rotation frequency at magnetic axis Ω is used as parameter for three sets of data. The growth rates for three rotation frequencies are nearly overlapped in the figure, although the growth rate with higher rotation is slightly larger than that with smaller rotation.

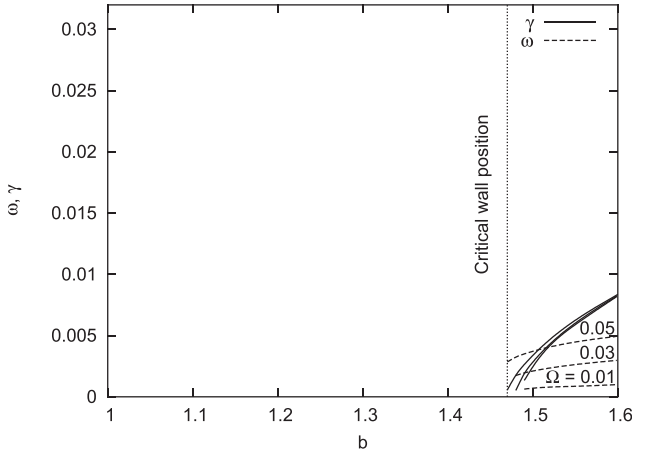

FIG. 8. The eigen frequency ω and growth rate γ versus the wall position b for the case with $q_p = 3.96$. The normalized rotation frequency at magnetic axis Ω is used as parameter for three sets of data. The three growth rate curves correspond the cases with $\Omega = 0.05$, 0.03, and 0.01 top-down.

Fig. 8. The real and imaginary eigen functions for the case with $q_p = 4.1$, $\Omega = 0.03$, $b = 1.33$, $\omega = -0.004965$, and $\gamma = 0.003618$ are plotted in Figs. 9 and 10. The real and imaginary eigen functions for the case with $q_p = 3.96$, $\Omega = 0.03$, $b = 1.48$, $\omega = -0.001737$, and $\gamma = -0.0005166$ are plotted in Figs. 11 and 12. The safety factor profiles and resonance surfaces are also indicated in these figures.

We first discuss the case with q_p larger than the integer number 4. Using Fig. 7 and the rotation profile, one can determine that the eigen mode frequency assumes the value of rotation frequency at q plateau on the side closer to the nearby resonance surface. This frequency is close to the rotation frequency at the pedestal top. This frequency range is consistent with the $n = 1$ EHO frequency observed experimentally.

Figure 7 shows that the eigen frequencies are insensitive to the wall position, while the growth rates do depend on it.

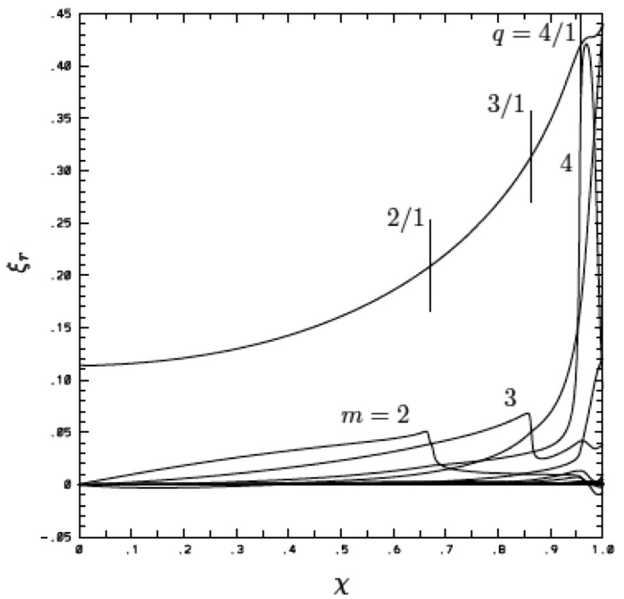

FIG. 9. The real part of eigenfunction versus normalized poloidal magnetic flux for the case with $q_p = 4.1$, $b = 1.33$, $\Omega = 0.03$, $\omega = -0.004965$, and $\gamma = 0.003618$.

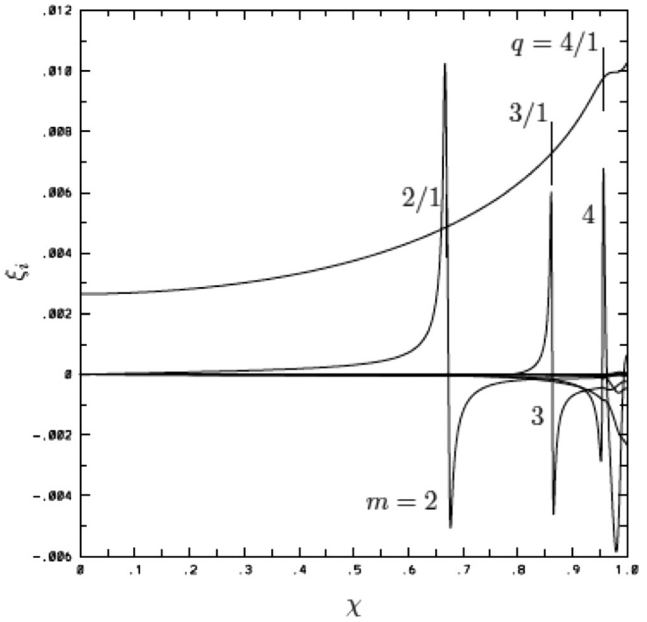

FIG. 10. The imaginary part of eigenfunction versus normalized poloidal magnetic flux for the case with $q_p = 4.1$, $b = 1.33$, $\Omega = 0.03$, $\omega = -0.004965$, and $\gamma = 0.003618$.

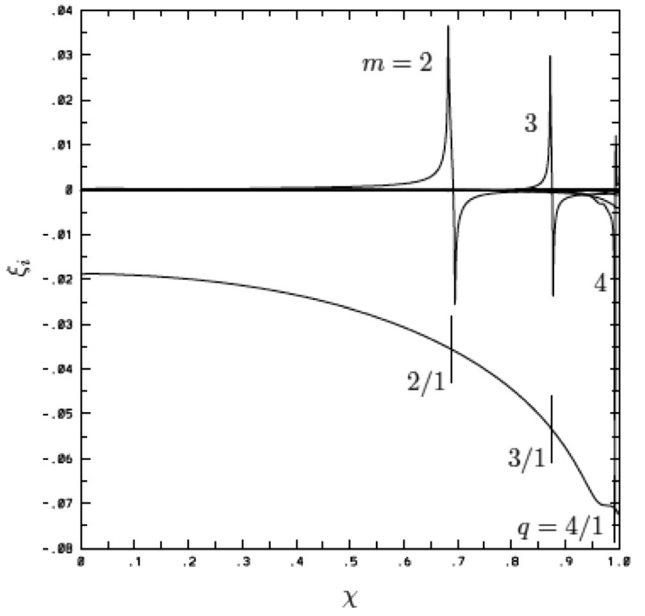

FIG. 12. The imaginary part of eigenfunction versus normalized poloidal magnetic flux for the case with $q_p = 3.96$, $b = 1.33$, $\Omega = 0.03$, $\omega = -0.001737$, and $\gamma = -0.0005166$.

This is because the mode frequencies tend to counter-match the rotation frequency for the $m = 4$ infernal harmonic. Since the rotation frequency is fixed, the eigen frequency remains constant. The wall position affects only the growth rate. We can use the cylindrical model to explain this. The singular layer equation for field line bending and inertia terms in this model can be written as follows:

$$\frac{d}{dr}\left[\left(\frac{1}{q}-\frac{n}{m}\right)^2-(\omega+n\Omega)^2\right]\frac{d\xi_m}{dr}\approx 0, \tag{4}$$

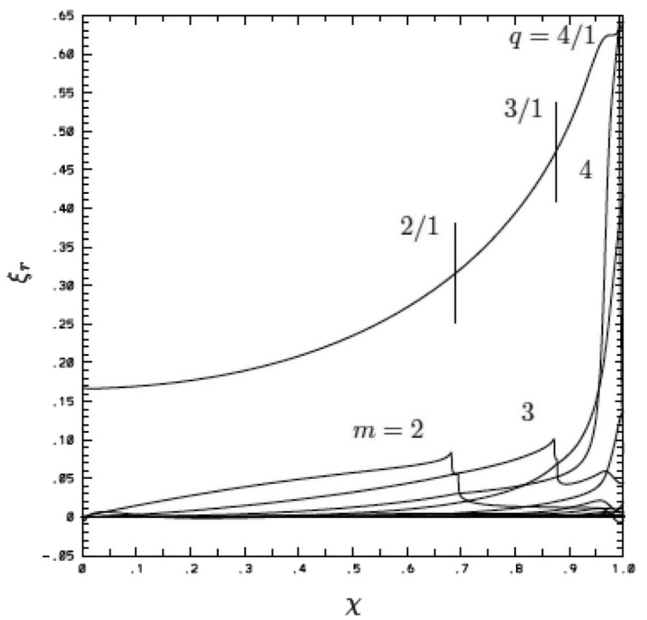

FIG. 11. The real part of eigenfunction versus normalized poloidal magnetic flux for the case with $q_p = 3.96$, $b = 1.48$, $\Omega = 0.03$, $\omega = -0.001737$, and $\gamma = -0.0005166$.

where r is the minor radius. From this equation, one can see that at the safety factor plateau the field line bending term becomes very small, as soon as the resonance surface $q = m/n$ is close to q_p. Therefore, the frequency of least stable mode tends to counter-match the rotation frequency (actually $n\Omega$) for $n = 1$ modes to minimize the rotation and field line bending stabilization effects. The extent of the frequency counter matching depends on how far q_p is from the rational number m/n for infernal harmonic. Since the $m = 4$ infernal mode energy dominates, the frequency counter matching occurs no matter wall position varies in the range specified in Fig. 7. The frequency insensitivity to wall position for $n = 1$ modes further confirms that the modes have the feature of infernal modes, instead of that of peeling-ballooning modes.

Figure 7 also shows that the growth rates for three different rotation frequencies remain basically the same. Note that in our equilibria, the rotation frequency varies radially, but the eigen frequencies have to be constant in the linear theory. From Eq. (4), one can see that the cancelation between the rotation frequency and eigen frequency cannot be made globally. However, in this case, the system stability is dominated locally by the $m = 4$ infernal branch, which peaks locally. The effects of different rotation frequencies are eliminated by the counter-matching mode frequencies. This local frequency cancellation tied to the $m = 4$ harmonic makes the growth rates in Fig. 7 to be roughly independent of rotation frequencies. The $m = 5$ peeling harmonic basically plays no role in determining the eigen mode frequency here. This is another indication that the modes are featured by the infernal type, instead of the peeling ballooning one.

Next, let us discuss the case with q_p less than the integer number 4. Figs. 8, 11, and 12 are for the $q_p = 3.96$ case. This case is not as typical of infernal type as the case with $q_p = 4.1$. This is because the 4/1 resonance surface for this

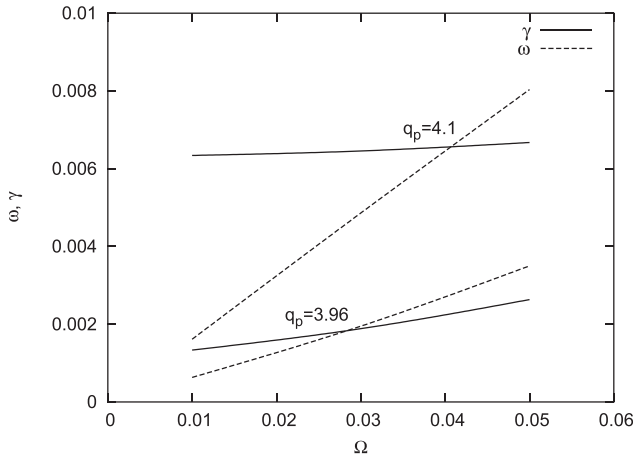

FIG. 13. The eigen frequency ω and growth rate γ versus the central rotation frequency Ω for two cases with q_p being specified.

case locates at pedestal foot and is closer to the plasma-vacuum interface. This closeness tends to induce the coupling of surface and vacuum energies—the peeling effects. Nonetheless, Fig. 8 shows that the infernal mode features still tend to prevail in this case: The eigen frequencies depend weakly on the wall position and the growth rates are almost independent of rotation frequencies.

To further demonstrate the infernal features of the modes, Figure 13 is given to show the dependence of eigen frequency and growth rate versus rotation frequencies for both the $q_p = 4.1$ and $q_p = 3.96$ cases. From this figure, one can see that the eigen frequencies varies linearly with the rotation frequency, but the growth rates basically remains constant. This is especially the case for the $q_p = 4.1$ case. This further confirms that there is a local cancellation of infernal type between the rotation and eigen frequencies.

We have also studied the rotation effects on the $q_p = 4.0$ case. This is the completely degenerated infernal mode case—i.e., the Mercier unstable case, as pointed out in the last section. The eigen modes in this case look like a delta function for single harmonic. Therefore, one can expect that the exact cancellation between the rotation and eigen modes frequencies occurs. This makes the dependence of eigen mode frequency on the rotation frequency is linear. The stability criterion becomes independent of rotation frequency.

Let us discuss a possible explanation for the excitation conditions for ELMs or EHOs. Figures 7, 8, and 13 show that the case with q_p larger than the integer number is more linearly unstable than the case with q_p smaller than the integer number. But, the case with q_p smaller than the integer number can be nonlinearly more damaging. Infernal modes are more localized and therefore are less coupled to external SOL current. They can help pump out plasma energy without causing ELMs.[17] This is exactly the role of EHOs in sustaining QH-mode discharges. Without releasing plasma energy, the equilibria with q_p smaller than the integer number can be further heated up, until it is suddenly corrupted, leading to the ELM bursts.

Experimental observations show that EHOs (or OMs) have wide, equal spacing frequency band: $n\omega$, corresponding to each Fourier modes of toroidal mode number n. We discuss a possible explanation for this based on the current infernal mode picture. Note that there is quasi-resonant nonlinear coupling phenomenon for infernal modes. Since the modes with higher toroidal mode number n are more localized, the local cancellation between the rotation and mode frequencies for $n = 1$ modes can also appear for higher n modes. Therefore, the linear eigen frequencies for modes with mode number n are close to the multiple of rotation frequency: $n\Omega$. Note further, for example, that the $n = 1$ modes with frequency ω can nonlinearly couple to become the nonlinear source for modes with $n = 2$ and frequency being 2ω. Since $\omega \approx \Omega$ for $n = 1$ case, the frequency of this source term nearly matches the linear eigen frequency of the $n = 2$ modes. Not only the frequencies match, the mode spatial locations are also nearly overlapped. This can cause the quasi-resonant nonlinear coupling. This may explain the experimental observations of wide, equal spacing frequency band of EHOs (or OMs). The nonlinear coupling in the infernal mode case is much stronger than the toroidal Alfvén mode (TAE) case, in which the double value of the 1st TAE frequency is usually not exactly the eigenfrequency for $n = 2$ TAE eigen frequency and the mode peak location varies.[25] The effects of linear local frequency cancellation and nonlinear quasi-resonant couplings may explain why the frequency band for EHO case is so wide, including more than 10 toroidal mode numbers sometimes. Using Eq. (4), we can find that the closer q_p to the rational number, the wider the resonant couplings by the dominant modes with the same resonance location, so that the wider the frequency band. For the $q_p = 4.1$ example, one can find that there is no additional rational surface between $q = 4/1$ and $q = 4.1$ surfaces for modes with mode number $n = 1, \cdots, 9$. Only in the $n = 10$ case 41/10 Fourier harmonic overtakes the 40/10 one as the dominant infernal harmonic.

Since an infernal mode is much more localized than a kink/peeling mode, it is reasonable to conjecture that the local pressure gradient near the plateau would flatten, as mode grows. This would saturate the mode, while leaving much of the pedestal gradient intact.

V. CONCLUSIONS AND DISCUSSION

In summary, we have studied the MHD instabilities of QH-mode pedestal with the inclusions of bootstrap current for equilibrium and rotation for stability in the JET-like equilibria. In view of the fact that QH mode is related to the low collisionality regime, we directly use the VMEC code with low collisonality bootstrap current model to construct the equilibria. We use the AEGIS code for stability investigation. In the numerical algorithm, we report the method to use the Cauchy-Riemann condition of dispersion relation to determine the unstable roots. This substantially extends beyond the commonly used Nyquist diagram method.

In the equilibrium calculation, we find that the inclusion of bootstrap current in the low collisionality regime can cause the safety factor to reverse or to form a plateau at the pedestal region. This confirms previous calculations with other codes.[6]

In the stability analyses, we find that the infernal harmonic can prevail in this type of equilibria. This is confirmed

by multiple facts, such as the eigenmode shape, mode position, as well as the independence of eigenmode frequency on the rotation frequency and wall position. The infernal type of harmonic is different from those of peeling-ballooning modes. The infernal harmonic tends to localize at safety factor plateau, while peeling-ballooning harmonics peak around respective resonance surfaces.

We find that the eigen mode frequency is close to the value of rotation frequency at pedestal top, when the value of safety factor at q plateau is slightly above an integer number. This frequency range is consistent with the $n=1$ EHO frequency observed experimentally. In the case with the value of safety factor being slightly lower than a rational number, the mode frequency tends to assume the rotation frequency close to but above the pedestal foot. Although the peeling effects have stronger influence on this case, the infernal mode features still tend to prevail. Although we have assumed that the rotation frequency has the same type of profile as the pressure one in our calculation, this conclusion seems to be insensitive to the details of the rotation profile shape, only the local rotation properties matter. This is because the cancellation between rotation and eigen frequencies is primarily a local phenomenon for these primarily localized modes.

We also point out that there is quasi-resonant nonlinear coupling phenomenon for infernal modes. The quasi-resonance can lead to local energy absorption and saturate the modes. The linear local cancellation between the rotation and eigen frequency, together with the overlap of mode locations, can induce the quasi-resonant nonlinear couplings. This may explain the wide, equal spacing frequency band observed experimentally for EHOs (or OMs).

We also find that the case with q_p larger than the integer number is more linearly unstable than the case with q_p smaller than the integer number. But, we point out that the case with q_p smaller than the integer number can be nonlinearly more damaging. Infernal modes can help pump out plasma energy without causing ELMs. They can play the role of EHOs in sustaining the QH-mode discharges. Without releasing plasma energy, the equilibrium with q_p smaller than the integer number can be further heated up, until it is finally corrupted, leading to the ELM bursts. This is a possible picture based on the infernal mode physics interpretation.

We also intend to study the more challenging cases with higher mode number and with finite Larmor radius effects being included. They will be investigated in the future.

ACKNOWLEDGMENTS

We would like to acknowledge Emilia R. Solano for helpful discussion. This research is supported by U. S. Department of Energy, Office of Fusion Energy Science.

[1]F. Wagner, G. Becker, K. Behringer, D. Campbell, A. Eberhagen, W. Engelhardt, G. Fussmann, O. Gehre, J. Gernhardt, G. V. Gierke, G. Haas, M. Huang, F. Karger, M. Keilhacker, O. Klüber, M. Kornherr, K. Lackner, G. Lisitano, G. G. Lister, H. M. Mayer, D. Meisel, E. R. Müller, H. Murmann, H. Niedermeyer, W. Poschenrieder, H. Rapp, H. Röhr, F. Schneider, G. Siller, E. Speth, A. Stäbler, K. H. Steuer, G. Venus, O. Vollmer, and Z. Yü, Phys. Rev. Lett. **49**, 1408 (1982).
[2]K. H. Burrell, W. P. West, E. J. Doyle, M. E. Austin, T. A. Casper, P. Gohil, C. M. Greenfield, R. J. Groebner, A. W. Hyatt, R. J. Jayakumar, D. H. Kaplan, L. L. Lao, A. W. Leonard, M. A. Makowski, G. R. McKee, T. H. Osborne, P. B. Snyder, W. M. Solomon, D. M. Thomas, T. L. Rhodes, E. J. Strait, M. R. Wade, G. Wang, and L. Zeng, Phys. Plasmas **12**, 056121 (2005).
[3]E. R. Solano, P. J. Lomas, B. Alper, G. S. Xu, Y. Andrew, G. Arnoux, A. Boboc, L. Barrera, P. Belo, M. N. A. Beurskens, M. Brix, K. Crombe, E. de la Luna, S. Devaux, T. Eich, S. Gerasimov, C. Giroud, D. Harting, D. Howell, A. Huber, G. Kocsis, A. Korotkov, A. Lopez-Fraguas, M. F. F. Nave, E. Rachlew, F. Rimini, S. Saarelma, A. Sirinelli, S. D. Pinches, H. Thomsen, L. Zabeo, and D. Zarzoso, Phys. Rev. Lett. **104**, 185003 (2010).
[4]P. B. Snyder, K. H. Burrell, H. R. Wilson, M. S. Chu, M. E. Fenstermacher, A. W. Leonard, R. A. Moyer, T. H. Osborne, M. Umansky, W. P. West, and X.Q. Xu, Nucl. Fusion **47**, 961 (2007).
[5]H. R. Wilson, S. C. Cowley, A. Kirk, and P. B. Snyder, Plasma Phys. Controlled Fusion **48**, A71 (2006).
[6]C. E. Kessel, G. Giruzzi, A. C. C. Sips, R. V. Budny, J. F. Artaud, V. Basiuk, F. Imbeaux, E. Joffrin, M. Schneider, M. Murakami, T. Luce, H. St John, T. Oikawa, N. Hayashi, T. Takizuka, T. Ozeki, Y.-S. Na, J. M. Park, J. Garcia, and A. A. Tucillo, Nucl. Fusion **47**, 1274 (2007).
[7]P. Zhu, C. C. Hegna, and C. R. Sovinec, Phys. Plasmas **19**, 032503 (2012).
[8]W. Wan, S. E. Parker, Y. Chen, Z. Yan, R. J. Groebner, and P. B. Snyder, Phys. Rev. Lett. **109**, 185004 (2012).
[9]S. Saarelma, T. Casper, I. T. Chapman, G. T. A. Huijsmans, O. Kwon, J. Lee, and A. Loarte, Nucl. Fusion **52**, 103020 (2012).
[10]J. Manickam, N. Pomphrey, and A. M. M. Todd, Nucl. Fusion **27**, 1461 (1987).
[11]F. L. Waelbroeck and R. D. Hazeltine, Phys. Fluids **31**, 1217–1223 (1988).
[12]T. C. Hender, S. J. Allfrey, B. Alper, Y. Baranov, D. N. Borba, D. Howell, G. T. A. Huysmans, O. J. Kwon, and M. Mantsinen, "MHD limiting JET optimised shear performance," EFDA-JET-PR(00)03 (2000).
[13]S. P. Hirshman and J. C. Whitson, Phys. Fluids **26**, 3553 (1983).
[14]L.-J. Zheng and M. Kotschenreuther, J. Comput. Phys. **211**, 748 (2006).
[15]L.-J. Zheng, M. Kotschenreuther, and M. S. Chu, Phys. Rev. Lett. **95**, 255003 (2005).
[16]H. Takahashi, E. D. Fredrickson, M. J. Schaffer, M. E. Austin, T. E. Evans, L. L. Lao, and J. G. Watkins, Nucl. Fusion **44**, 1075 (2004).
[17]L. J. Zheng, H. Takahashi, and E. D. Fredrickson, Phys. Rev. Lett. **100**, 115001 (2008).
[18]D. A. Spong, S. P. Hirshman, L. A. Berry, J. F. Lyon, R. H. Fowler, D. J. Strickler, M. J. Cole, B. N. Nelson, D. E. Williamson, A. S. Ware, D. Alban, R. Snchez, G. Y. Fu, D. A. Monticello, W. H. Miner, and P. M. Valanju, Nucl. Fusion **41**, 711 (2001).
[19]K. C. Shaing, E. C. Crume, J. S. Tolliver, S. P. Hirshman, and W. I. van Rij, Phys. Fluids B **1**, 148 (1989).
[20]M. Landreman and D. R. Ernst, Plasma Phys. Controlled Fusion **54**, 115006 (2012).
[21]F. L. Waelbroeck and L. Chen, Phys. Fluids B **3**, 601 (1991).
[22]L.-J. Zheng, M. S. Chu, and L. Chen, Phys. Plasmas **6**, 1217 (1999).
[23]J. M. Greene and J. L. Johnson, Phys. Fluids **5**, 510 (1962).
[24]E. Chen, H. Berk, B. Breizman, and L. J. Zheng, Bull. Am. Phys. Soc. **55**, 277 (2010).
[25]H. Smith, B. N. Breizman, M. Lisak, and D. Anderson, Phys. Plasmas **13**, 042504 (2006).